SINERGI Vol. 27, No. 1, February 2023: 15-22
http://publikasi.mercubuana.ac.id/index.php/sinergi
http://doi.org/10.22441/sinergi.2023.1.003

Finite Element Analysis on ballistic impact performance of multi-layered bulletproof vest impacted by 9 mm bullet

Azhari Sastranegara[1], Kevin Eka Putra[1], Edmun Halawa[1], Nanang Ali Sutisna[1], Ameen Topa[2]
[1]Department of Mechanical Engineering, Faculty of Engineering, President University, Indonesia
[2]Department of Maritime Technology, Faculty of Ocean Engineering Technology and Informatics, Universiti Malaysia Terengganu, Malaysia

Abstract
Simulation is one of the most effective ways to reduce the cost and time needed to test the quality of a bulletproof vest. The widely applied method to predict the behavior of the materials is a macro-homogeneous model. However, even though it is low in computational cost, it has some accuracy issues. This work presents finite element analysis with both macro-homogeneous and meso-heterogeneous models to predict the behavior of the Kevlar composites during ballistic impact and qualitatively compares the simulation results with the experimental ones. The simulation reliability was ensured by numerical parameters such as the system energy balance and the limitation of artificial energy. The simulation results showed that the meso-heterogeneous yarn model successfully produced more detailed impact damage than the macro-homogenous model. In addition, the deformation of the Kevlar, the bullet, and the steel plate was close to the experiment results. The result was expected to be used as a consideration in determining the model type for another similar research.

Keywords:
Ballistic impact test;
Macro-homogenous model;
Meso-heterogenous model;
Numerical analysis;

Article History:
Received: March 9, 2022
Revised: August 24, 2022
Accepted: September 14, 2022
Published: February 2, 2023

Corresponding Author:
Azhari Sastranegara,
Mechanical Engineering Department, President University, Indonesia
Email: azhari.sastranegara@president.ac.id

INTRODUCTION

Numerous types of armor have been created throughout the history of body armor, from leather to a vest that protects the torso, which is widely used nowadays. The materials used are also different. During the early wars, most of them were made from metal plates. Although metal plate armor gives enough protection to the wearer, it is considerably heavy, so metal is not compatible with the soldiers' mobility. Nowadays, the primary consideration of body armor is its wearing flexibility and its ability to absorb the impact from the ballistic projectile. Though giving complete protection to the wearer is practically impossible, engineers and scientists made choices in making body armor. The protection of another part of the body armor will be traded off to enhance protection in a specific part [1, 2, 3].

In the process of body armor development, ballistic impact testing is applied to test the ability of the material to absorb the impact from the projectile. The ballistic impact testing shows us the phenomenon of a projectile hitting the targeted vest. However, the testing costs a lot of money and time. Therefore, an accurate numerical analysis is needed to cut the computational cost required [4, 5, 6].

Creating a numerical model of ballistic impact requires the appropriate choices for several features. Model scale and the boundary conditions assumption are crucial, but the most important key point is the choice of the constitutive material models and the related parameters. While the modeling of metal armor is relatively mature, it is not the case for composite fabric like Kevlar. Two prominent techniques have been employed in the literature, each with advantages.

The first technique does not simulate every yarn and the matrix but considers a layer as a homogenous sheet with comparable mechanical properties. This technique is often referred to as the Macro-homogenous model. This method has the advantages of simplicity and low computing cost. The second technique, the Meso-heterogeneous model, instead simulates every single yarn, the epoxy matrix, and the interaction among them. This approach provides a more detailed analysis of fabric behavior, but as a consequence, it requires a more expensive computing cost [7, 8, 9].

The current work presents a numerical study of the ballistic resistance of a commercial bulletproof vest consisting of several Kevlar layers and a steel plate subjected to a 9 mm caliber projectile impact [10], and some previous articles which has a similar type of analysis [11, 12, 13]. This vest is a type IV bulletproof vest used by the Indonesian Army (TNI-AD). The numerical models are developed using explicit finite element code LS-DYNA® with Macro-homogenous and Meso-heterogeneous approaches without modeling the epoxy matrix. The validity of the simulations is evaluated by assessing the numerical stability and qualitatively comparing the results to the experiment.

METHOD

This research will use the Finite Element Method to analyze the ballistic experiment [14, 15, 16]. Then, the researcher will compare the macro-homogenous and meso-heterogeneous from the numerical stability aspect and compare both models' results to the experiment results.

Experimental Condition

The vest is 13.1 mm thick, and made of 11 layers of bulletproof fabric and one bulletproof steel plate, as illustrated in Figure 1. The fabric is impregnated in an Epoxy matrix and is a 2D plain-weave. The 9 mm projectile was fired from an STI Edge pistol with an initial speed of approximately 370 m/s perpendicularly to the vest. The firing distance is 5 meters, following the standard of NIJ0101.06. The experiment was conducted at the Indonesian Army firing range with professional assistance from the army personnel. The firing test layout is described in Figure 2.

The material benchmark revealed that the vest parts consisted of fabric and steel plates, as listed in Table 1. The bullet illustration is shown in Figure 3. It is a full metal jacket with round-nose bullet. Its materials are Brass 72 (CuZn28) for the jacket and Lead Antimony for the core metal.

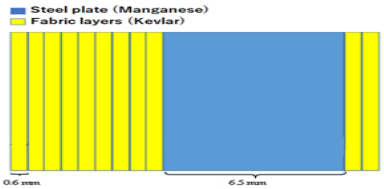

Figure 1. The vest's layers structure

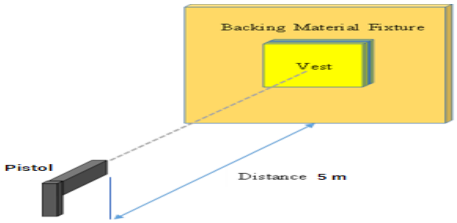

Figure 2. The firing experiment setup

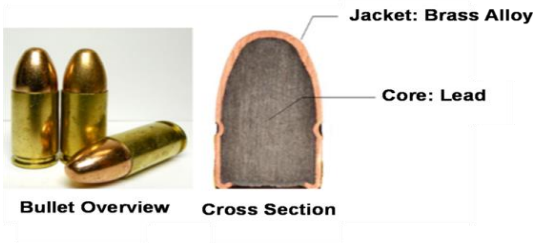

Figure 3. The Firing Experiment Setup Illustration

Table 1. Vest components' thickness

Part Name	Material	Thickness	Remarks
Fabric Layers	Kevlar	0.6 mm	11 layers
Steel Plate	Manganese Steel	6.5 mm	1 plate

Numerical Model

The simulation was run in LS-Dyna®, and all the analyses adopted the explicit method approach as a widespread technique in analyzing the non-linear phenomenon and large deformation [7, 8, 14]. The energy ratio criterion was implemented to evaluate the acceptability of the simulation. The criterion rules that the system's total energy should remain constant during the impact. Hence, throughout the simulation, the ratio between total energy, initial kinetic energy, and work of the external forces should be as close as possible to one, with the maximum acceptable difference of 5%.

The Kevlar layers in the macro-homogeneous model used shell elements; on the other hand, in the meso-heterogeneous, the solid elements are used. The steel plate and the bullet are modeled using solid elements considering the temperature rise effect and shock-compressed solid, represented by applying the Johnson-Cook model and the EOS Gruneisen. In this simulation, the epoxy matrix part is not modeled since its strength compared to the Kevlar yarn is

considerably small, less than 5% of Kevlar's [6]. The macro-homogenous and meso-heterogeneous finite element models of the vest and bullet are shown in Figure 4 and Figure 5. Since the models are symmetrical, the quarter model is applied for calculation efficiency.

The yarn model was constructed using TexGen®, an open-source software developed at the University of Nottingham. The yarn dimension is shown in Figure 6, while the yarn meshing and assembling are shown in Figure 7 and Figure 8.

Mechanical Properties of the Composite

The Kevlar properties are chosen from Kevlar®29 since this is the most used type in the modern bulletproof vest. The damaged mode is applied in the solver using the keyword MAT_ADD_EROSION, with the maximum strain ɛf and the ultimate tensile strength as the criterion of failure for the Kevlar woven. The MAT_ADD_EROSION allows failure and erosion to be expressed in the constitutive model [17].

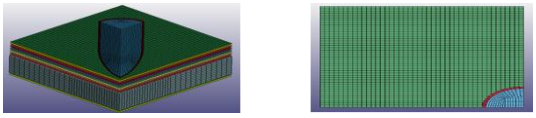

Figure 4. Macro-homogenous vest model

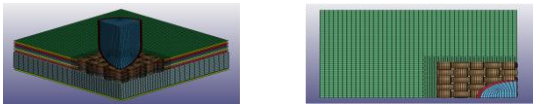

Figure 5. Meso-heterogenous vest model

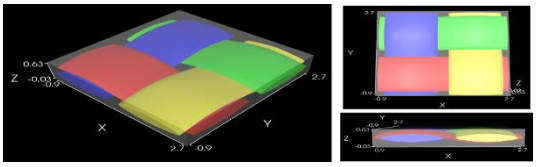

Figure 6. Yarn Construction using TexGen®

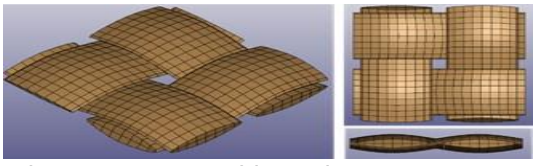

Figure 7. Yarn meshing using LS-PrePost®

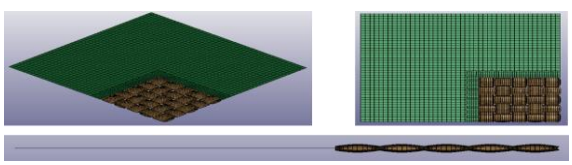

Figure 8. Assembling of the Meso-heterogeneous model

The element will be deleted from the calculation once the strain reaches the criterion. This keyword is recommended to prevent large deformation in the elements, which might cause numerical instabilities [18].

The meso-heterogeneous model considers each yarn as an elastic material. In LS-Dyna, this material is represented by the MAT_ELASTIC model. This model is available for beam, shell, and solid, which suits the yarns modeled as solid [19]. The following equations are the force resultant in (1) and the moment resultant in (2) of the material model.

$$F_i^{n+1} = F_i^n + \left(1 + \frac{\mathrm{DA}}{\Delta \mathrm{t}}\right) \Delta F_i^{n+\frac{1}{2}} \quad (1)$$

$$M_i^{n+1} = M_i^n + \left(1 + \frac{\mathrm{DB}}{\Delta \mathrm{t}}\right) \Delta M_i^{n+\frac{1}{2}} \quad (2)$$

In the macro-homogenous model, the woven constructed of yarns is considered one homogenous material sheet. The material model used to represent the Kevlar woven is MAT_ENHANCED_COMPOSITE_DAMAGE is commonly used as it does not require complicated input parameters [20][21]. Therefore, this material model was adopted to represent the Kevlar woven. In addition, the model is suitable for shell elements to model transverse shear deformation and the constant shear strain through the thickness of the shell. The properties are referred to from the literature [8] and presented in Table 2.

The material model has a tensile failure criterion for fiber mode, as shown in (3), the compressive criterion for fiber mode shown in (4), and the failure criterion for both tensile and compressive matrix model shown in (5).

Table 2. Kevlar hetero-homogenous properties

Property	Value	Unit
Density, ρ	1.440e-09	Ton.mm^{-3}
Young's Modulus, E	8.30e+04	MPa
Poisson's Ratio, υ	0.44	-
Ultimate Tensile Strength, σ_f	3620	MPa
Maximum Strain, ε_f	4.4	%
Property	Value	Unit

$$e_f^2 = \left(\frac{\sigma_{11}}{X_t}\right)^2 + \left(\frac{\sigma_{12}}{S_c}\right)^2 - 1 \begin{cases} \geq 0 \text{ failed} \\ < 0 \text{ elastic} \end{cases} \quad (3)$$

$$e_c^2 = \left(\frac{\sigma_{11}}{X_c}\right)^2 - 1 \begin{cases} \geq 0 \text{ failed} \\ < 0 \text{ elastic} \end{cases} \quad (4)$$

$$e_{md}^2 = \frac{\sigma_{22}^2}{Y_c Y_t} + \left(\frac{\sigma_{12}}{S_c}\right)^2 + \frac{(\mathrm{Yc} - \mathrm{Yt})\sigma_{22}}{Y_c Y_t} - 1 \begin{cases} \geq 0 \text{ failed} \\ < 0 \text{ elastic} \end{cases} \quad (5)$$

Table 3. Kevlar macro-homogenous properties

Material Property	Value	Unit
Density, ρ	1.440e-09	MPa
Young's Modulus longitudinal, EA	1.850e+04	MPa
Young's Modulus transverse, EB	1.850e+04	MPa
Young's Modulus average, EC	6000	MPa
Poisson's Ratio, υBA	0.25	-
Poisson's Ratio, υCA, υCB	0.33	-
Shear Modulus, GAB	770	MPa
Shear Modulus, GBC, GCA	5430	MPa
Longitudinal compressive strength, XC	185	MPa
Longitudinal tensile strength, XT	1850	MPa
Transverse compressive strength, YC	185	MPa
Transverse tensile strength, YT	1850	MPa
Shear strength, SC	77	MPa

Mechanical Properties of the Composite

The steel plate is made of manganese steel alloy close to Weldox 700E properties. Therefore, the values inputted in the selected material model MAT_MODIFIED_ JOHNSON_COOK refer to the Weldox 700 properties listed in Table 4 [22]. The MAT_MODIFIED_JOHNSON_COOK is suitable for adiabatic heating [23]. However, since the bullet will not severely impact the steel plate, it is better to use the modified version of the Johnson cook constitutive model.

The bullet-model is made as a 9mm bullet, as shown in Figure 9. The material used is brass as the jacket and lead as its core. The material properties used are presented in Table 5. The brass and lead are set to erode in contact when the criteria are satisfied. To correctly simulate this behavior, the keyword of ERODING_SURFACE_TO_SURFACE is used.

The brass and lead of the bullet adopt the Johnson-Cook constitutive model with the properties and variables listed in Table 5 and Table 6 [7, 24, 25]. The Gruneisen equation is used to make a threshold for the strain rate during the compression of the bullet. The Gruneisen EOS parameters used are listed in Table 7 [7].

The material model of MAT_ JOHNSON_ COOK has the strain and temperature-sensitive plasticity used for problems where the strain rates vary over an extensive range.

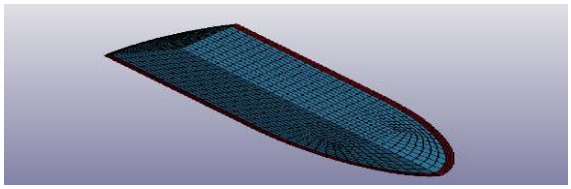

Figure 9. The 9mm bullet-model

There is also an adiabatic temperature increase caused by plastic heating, which results in material softening. Following are the equations for the MAT_JOHNSON_COOK's flow stress.

$$\sigma_y = \left(A + B\bar{\varepsilon}^{p^n}\right)(1 + c\ln\dot{\varepsilon}^*)\left(1 - \mathrm{T}^{*^m}\right) \qquad (6)$$

Where A, B, C, n, and m are input constants, $\bar{\varepsilon}^p$ is the effective plastic strain, $\dot{\varepsilon}^*$ is the normalized effective plastic strain rate, and T* for the homologous temperature.

$$\left(T^* = \frac{T - T_{room}}{T_{melt} - T_{room}}\right) \qquad (7)$$

Table 4. Properties of steel

Material Property	Value	Unit
Density, ρ	7.850 e-09	Ton.mm^{-3}
Young's Modulus, E	2.100 e+05	MPa
Poisson's Ratio, υ	0.33	-
Taylor-Quinney Coefficient	0.9	-
Specific Heat, Cp	4.520 e+08	J.kg^{-1} K^{-1}
Expansion Coefficient, α	1.200 e-05	K^{-1}
Zerilli-Armstrong parameter, A	819	MPa
Zerilli-Armstrong parameter, B	308	MPa
Zerilli-Armstrong parameter, N	0.64	-
Zerilli-Armstrong parameter, C	0.0098	-
Reference Strain Rate, $(\varepsilon\_0)^{\cdot}$	5.000 e-04	s^{-1}
Room Temperature, Tr	293	K
Melt Temperature, Tm	1800	K
J-C thermal softening, m	1	-
Failure Criterion, Wcr	1486	MPa

Table 5. General properties of the bullet

Property	Lead	Brass	Unit
Density	1.066e-08	8.520e-09	Ton / mm^3
Young's Modulus	1.800e+04	1.150e+05	MPa
Poisson's Ratio	0.42	0.31	-
Shear Modulus	4900	4.000e+04	MPa

Table 6. Johnson-Cook parameters of the bullet

Property	Lead	Brass	Unit
A	1	111.69	MPa
B	55.551	504.69	MPa
N	0.098	0.42	-
C	0.230	0.009	-
M	1	1.68	-
D1	-	0.00	-
D2	-	2.65	-
D3	-	-(0.62)	-
D4	-	0.028	-
D5	-	0.00	-
TM	760	988	K
TR	293	293	K
$\dot{\varepsilon}_0$	5.000e-04	5.000e-04	s-1
Cp	1.240e+10	3.850e+10	N mm / Ton K

Table 7. Gruneisen EOS parameter of bullet

Property	Lead	Brass	Unit
C	2.028e+06	3.834e+06	Mm/s
S1	1.627	1.429	-
γ_0	2.253	2.000	-

RESULTS AND DISCUSSION

In this section, the simulation results of Macro-Homogenous and Meso-Heterogenous will be presented consecutively.

Numerical Model Evaluation

The model's validity from the viewpoint of numerical stability is evaluated from the total energy, which consists of the kinetic energy, and internal energy, as shown in Figure 10 and Figure 11. The next indicator of stability is the system's energy ratio, which should be near the value of one throughout the simulation, as shown in Figure 12 and Figure 13. Lastly, the energy generated from the hourglass mode is also evaluated to ensure that the model results do not contain too much artificial energy, as shown in Figure 14 and Figure 15.

The result shows that the total energy is constant throughout the simulation. The artificial energy is less than 10%, which is widely considered the acceptable limit for the artificial energy introduced in simulation.

From the results above, it can be concluded that both the macro-homogeneous and meso-heterogeneous models have good numerical stability. Thus, both models presented here are reliable in terms of numerical performance. Therefore, the following evaluation will compare the simulation results and the experiment.

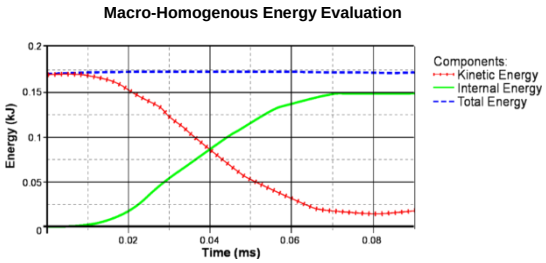

Figure 10. Macro-homogeneous Energy

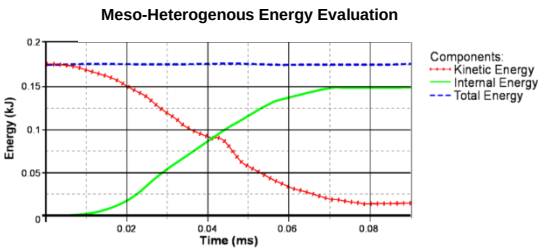

Figure 11. Meso-heterogeneous Energy

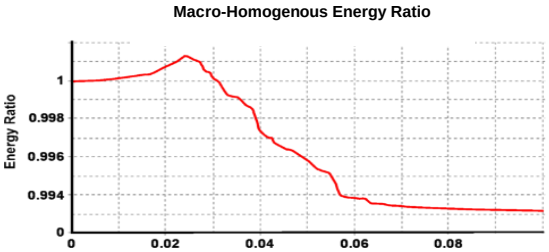

Figure 12. Macro-homogeneous history of the energy ratio

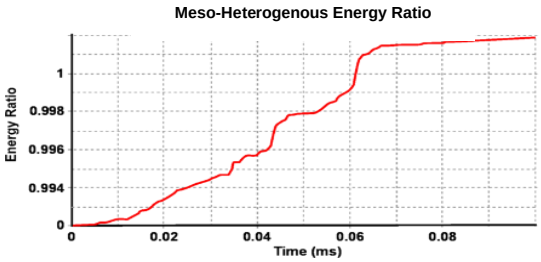

Figure 13. Meso-heterogeneous history of the energy ratio

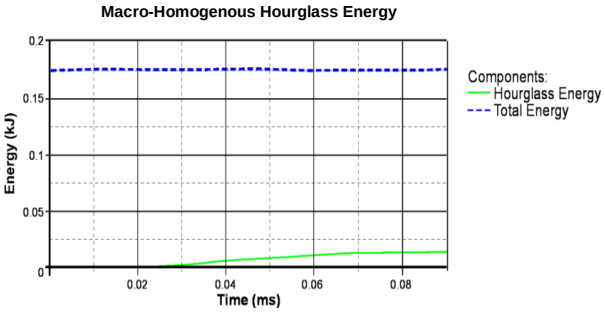

Figure 14. Macro-homogeneous history of the hourglass energy

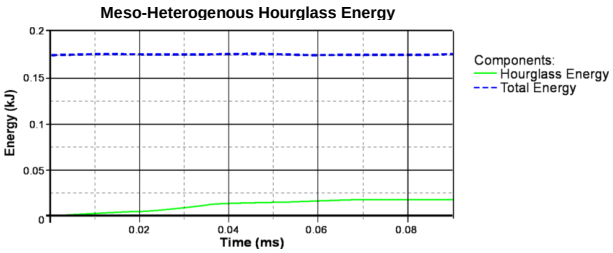

Figure 15. Meso-heterogeneous history of the hourglass energy

Visual Comparison

The simulation results will be compared to the experimental results qualitatively. Figure 16 shows the final results from both macro-homogeneous and meso-heterogeneous through the simulation. The processes' representation for both models will also be displayed in Table 8. The computational cost from the macro-homogeneous model was lower than the cost of the meso-heterogeneous model. The macro-homogeneous

model calculation was approximately 12 times faster than the meso-heterogeneous model, using a personal computer with an Intel Core i5-7200U and 12 GB RAM.

Table 9 compares the macro-homogenous and the meso-heterogeneous simulation results to the experiment from each of the Kevlar layers, the steel plate, and the bullet's deformation. We can see that the macro-homogeneous model gave us the overall impact damage results from the bullet. Still, the damage is pictured more detailed in the meso-heterogeneous model. The damage of the steel plate shown by the macro-homogeneous and the meso-heterogeneous models have a similar area of impact to the experiment result.

Lastly, the bullet deformation result from meso heterogeneous is closer to the experiment than the macro-homogeneous bullet. Therefore, it seems that the macro-homogenous model has limitations in modeling the deformation of Kevlar sheets from the early stage.

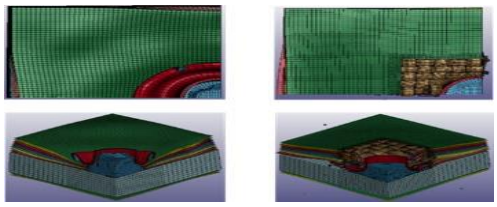

Figure 16. homogeneous (left) and Meso-heterogeneous (right).

Table 8. Simulation time-steps

Macro-homogeneous model	Meso-heterogeneous model
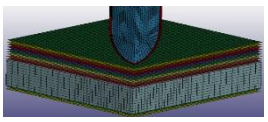 0 ms	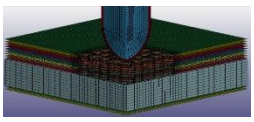 0 m
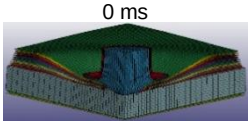 0.04 ms	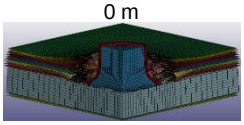 0.04 ms
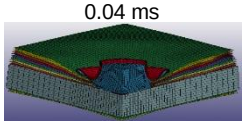 0.06 ms	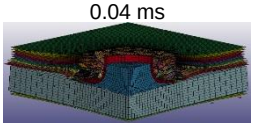 0.06 ms
 0.1 ms	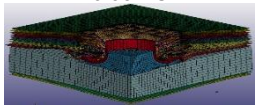 0.1 ms

Table 9. Comparison of Numerical Analysis Results toward Experimental Results

No.	Macro homogenous	Experiment	Meso heterogenous
1			
2			
3			
4			
5			
6			
7			
8			
9			
10			
11			

The results show that the impact damage simulated by both models is acceptable compared to the experiment results. However, the meso-heterogeneous model gives more detailed damage information of the composite layers. Both models represent the damage with the size close enough to the experimental results for the steel plate.

The meso-heterogenous model simulated the deformation closer to the experimental result than the macro-homogeneous model for the final bullet deformation. Lastly, the 2 Kevlar layers behind the steel plate were not damaged, as the penetration stopped right at the steel plate.

CONCLUSION

The numerical analysis was done in both macro-homogeneous and meso-heterogeneous models. The computational cost of the meso-heterogeneous was almost 12 times higher than the macro-homogeneous model. Both models showed acceptable physical parameters such as energy balance and energy ratio. While the hourglass energy of the meso-heterogeneous is slightly higher than the macro-homogeneous, both of the models were able to keep the hourglass energy below 10%. However, the meso-heterogeneous model was more realistic than the macro-homogenous one. The deformation of Kevlar in macro-homogenous mentioned it was getting smaller on the last layer, which showed that the Kevlar was too tough. In fact, the deformation should be getting bigger, refer to previous research.

The future work of the numerical analysis on the ballistic impact performance of multi-layered bulletproof vests can be done using different bullets based on different backgrounds for military or defence purposes. This work still has a lot of room for improvement, such as the composite detail can be improved to model the yarn along with the epoxy matrix or a complete composite model using the meso-heterogeneous model. This can be achieved by providing a high-performance computation machine. Furthermore, to better understand the impact of bullets on the vest, it is necessary to provide a speed detector and a high-speed camera to capture the details. Future works using different materials and models can also be done to predict the behavior of different alternative vests to obtain a better vest composite. Lastly, quantitative research regarding the vest's ability to absorb the damage and a better composite structure to absorb and stop the bullet from penetrating is highly recommended.

ACKNOWLEDGMENT

This research was supported by PT. Perisai Inti Sejahtera. We thank our colleagues from President University who provided insight and expertise that greatly assisted the research despite their not agreeing with some parts of the interpretations and conclusions of this paper.

REFERENCES

[1] P. J. Hazell, *Armour, Materials, Theory, and Design*, Boca Raton: CRC Press, 2022, doi: 10.1201/9781003322719.

[2] M. A. Abtew, F. Boussu, and P. Bruniaux, "Dynamic impact protective body armour: A comprehensive appraisal on panel engineering design and its prospective materials," *Defence Technology*, vol. 17, no. 6, pp. 2027–2049, Dec. 2021, doi: 10.1016/j.dt.2021.03.016.

[3] N. Kumar, "Bulletproof Vest and Its Improvement - A Review," *International Journal of Scientific Development and Research*, vol. 1, no. 1, pp. 34–39, Jan. 2016.

[4] D. Weerasinghe, M. R. Bambach, D. Mohotti, H. Wang, S. Jiang, and P. J. Hazell, "Development of a Coated Fabric Armour System of Aramid Fibre and Rubber," *Thin-Walled Structures*, vol. 179, p. 109679, Oct. 2022, doi: 10.1016/j.tws.2022.109679.

[5] H. Wang et al., "On the impact response of UHMWPE woven fabrics: Experiments and simulations," *International Journal of Mechanical Sciences*, vol. 204, p. 106574, Aug. 2021, doi: 10.1016/j.ijmecsci.2021.106574.

[6] D. Weerasinghe, D. Mohotti, and J. Anderson, "Numerical Modelling of the Rate-sensitive Behaviour of High-performance Fabrics," *Journal of Dynamic Behavior of Materials*, vol. 7, no. 1, pp. 107–126, Mar. 2021, doi: 10.1007/s40870-020-00274-4.

[7] L. M. Bresciani, A. Manes, A. Ruggiero, G. Iannitti, and M. Giglio, "Experimental tests and numerical modelling of ballistic impacts against Kevlar 29 plain-woven fabrics with an epoxy matrix: Macro-homogeneous and Meso-heterogeneous approaches," *Composites Part B: Engineering*, vol. 88, pp. 114–130, Mar. 2016, doi: 10.1016/j.compositesb.2015.10.039.

[8] R. Scazzosi, A. Manes, G. Petrone, and M. Giglio, "Two different modelling approaches for fabric composites subjected to ballistic impact," *IOP Conference Series: Materials Science and Engineering*, vol. 406, p. 012051, Sep. 2018, doi: 10.1088/1757-899X/406/1/012051.

[9] L. A. Bokhoeva, A. B. Baldanov, V. E. Rogov, A. S. Chermoshentseva, and T. Ameen, "The effect of the addition of nanopowders on the strength of multilayer composite materials," *Industrial laboratory. Diagnostics of materials*, vol. 87, no. 8, pp. 42–50, Aug. 2021, doi: 10.26896/1028-6861-2021-87-8-42-50.

[10] A. Sastranegara, E. Halawa, and L. Anggraini, "Experimental study on the performance of multi-layered bulletproof vest," *SINERGI*, vol. 26, no. 3, p. 287, Oct. 2022, doi: 10.22441/sinergi.2022.3.003.

[11] S. Li, J.-S. Yang, L.-Z. Wu, G.-C. Yu, and L.-J. Feng, "Vibration behavior of metallic sandwich panels with Hourglass truss cores," *Marine Structures*, vol. 63, pp. 84–98, Jan. 2019, doi: 10.1016/j.marstruc.2018.09.004.

[12] S. S. Asemani, G. Liaghat, H. Ahmadi, Y. Anani, A. Khodadadi, and S. C. Charandabi, "The experimental and numerical analysis of the ballistic performance of elastomer matrix Kevlar composites," *Polymer Testing*, vol. 102, p. 107311, Oct. 2021, doi: 10.1016/j.polymertesting.2021.107311.

[13] G. Guo, S. Alam, and L. D. Peel, "Numerical analysis of ballistic impact performance of two ceramic-based armor structures," *Composites Part C: Open Access*, vol. 3, p. 100061, Nov. 2020, doi: 10.1016/j.jcomc.2020.100061.

[14] J. Mueller, K. H. Matlack, K. Shea, and C. Daraio, "Energy Absorption Properties of Periodic and Stochastic 3D Lattice Materials," *Advanced Theory and Simulations*, vol. 2, no. 10, p. 1900081, Oct. 2019, doi: 10.1002/adts.201900081.

[15] global sci, "Multigrid Method for Poroelasticity Problem by Finite Element Method," *Advances in Applied Mathematics and Mechanics AAMM*, vol. 11, no. 6, pp. 1339–1357, Jun. 2019, doi: 10.4208/aamm.OA-2019-0003.

[16] X. Zhang, T. Liu, N. He, and G. Jia, "Investigation of two finite element modelling approaches for ballistic impact response of composite laminates," *International Journal of Crashworthiness*, vol. 22, no. 4, pp. 377–393, Jul. 2017, doi: 10.1080/13588265.2016.1270495.

[17] A. Dua, A. Braimah, and M. Kumar, "Experimental and numerical investigation of rectangular reinforced concrete columns under contact explosion effects," *Engineering Structures*, vol. 205, p. 109891, Feb. 2020, doi: 10.1016/j.engstruct.2019.109891.

[18] Q. H. Shah and A. Topa, "Modeling Large Deformation and Failure of Expanded Polystyrene Crushable Foam Using LS-DYNA," *Modelling and Simulation in Engineering*, vol. 2014, pp. 1–7, 2014, doi: 10.1155/2014/292647.

[19] A. Apuzzo, R. Barretta, R. Luciano, F. Marotti de Sciarra, and R. Penna, "Free vibrations of Bernoulli-Euler nano-beams by the stress-driven nonlocal integral model," *Composites Part B: Engineering*, vol. 123, pp. 105–111, Aug. 2017, doi: 10.1016/j.compositesb.2017.03.057.

[20] E. Gungor, A. Topa, and B. O. Kucukyildirim, "Numerical Investigation of Innovative Honeycomb-Composite Sandwich Structure Under Bird-Strike Event," in *6th International Conference On Advances In Mechanical Engineering Istanbul*, Oct. 2021.

[21] M. N. M. Ansari, K. S. Vinoth, A. Nordin, A. Bassam, and A. Topa, "Tensile properties of hybrid kenaf/glass fiber reinforced epoxy composites with different stacking sequence using experimental and FEA simulation method," *IOP Conference Series: Materials Science and Engineering*, vol. 1128, no. 1, p. 012023, Apr. 2021, doi: 10.1088/1757-899X/1128/1/012023.

[22] C. Özorak, F. Okay, E. Özorak, and S. Islak, "Wear and microstructural properties of coatings on Weldox 700 steel," *Materials Testing*, vol. 62, no. 6, pp. 645–651, Jun. 2020, doi: 10.3139/120.111526.

[23] B. Song and B. Sanborn, "A Modified Johnson–Cook Model for Dynamic Response of Metals with an Explicit Strain- and Strain-Rate-Dependent Adiabatic Thermosoftening Effect," *Journal of Dynamic Behavior of Materials*, vol. 5, no. 3, pp. 212–220, Sep. 2019, doi: 10.1007/s40870-019-00203-0.

[24] A. Bracq, J.-S. Brest, J. A. de Sampaio, F. Moitrier, and Y. Demarty, "Characterization and modelling of the mechanical behaviour of metal rings: Application to a brass bullet jacket," *Forces in Mechanics*, vol. 4, p. 100030, Oct. 2021, doi: 10.1016/j.finmec.2021.100030.

[25] M. Boldyrev, "Lead: properties, history, and applications," *WikiJournal of Science*, vol. 1, no. 2, p. 7, Jul. 2018, doi: 10.15347/wjs/2018.007.